UCLA
UCLA Previously Published Works

Title
Conformational Dynamics of Amyloid β-Protein Assembly Probed Using Intrinsic Fluorescence †

Permalink

Journal
Biochemistry, 44(40)

ISSN
0006-2960

Authors
Maji, Samir K
Amsden, Jason J
Rothschild, Kenneth J
et al.

Publication Date
2005-10-01

DOI
10.1021/bi0508284

Peer reviewed

Conformational Dynamics of Amyloid β-Protein Assembly Probed Using Intrinsic Fluorescence[†]

Samir K. Maji,[‡] Jason J. Amsden,[§] Kenneth J. Rothschild,[§] Margaret M. Condron,[‡] and David B. Teplow*[,‡]

*Department of Neurology, David Geffen School of Medicine at UCLA, Los Angeles, California 90095, and Department of
Physics, Molecular Biophysics Laboratory, Boston University, Boston, Massachusetts 02215*

Received May 4, 2005; Revised Manuscript Received July 7, 2005

ABSTRACT: Formation of toxic oligomeric and fibrillar structures by the amyloid β-protein (Aβ) is linked to Alzheimer's disease (AD). To facilitate the targeting and design of assembly inhibitors, intrinsic fluorescence was used to probe assembly-dependent changes in Aβ conformation. To do so, Tyr was substituted in Aβ40 or Aβ42 at position 1, 10 (wild type), 20, 30, 40, or 42. Fluorescence then was monitored periodically during peptide monomer folding and assembly. Electron microscopy revealed that all peptides assembled readily into amyloid fibrils. Conformational differences between Aβ40 and Aβ42 were observed in the central hydrophobic cluster (CHC) region, Leu^{17}−Ala^{21}. Tyr^{20} was partially quenched in unassembled Aβ40 but displayed a significant and rapid increase in intensity coincident with the maturation of an oligomeric, α-helix-containing intermediate into amyloid fibrils. This process was not observed during Aβ42 assembly, during which small decreases in fluorescence intensity were observed in the CHC. These data suggest that the structure of the CHC in Aβ42 is relatively constant within unassembled peptide and during the self-association process. Solvent accessibility of the Tyr ring was studied using a mixed solvent (dimethyl sulfoxide/water) system. [Tyr^{40}]Aβ40, [Tyr^{30}]Aβ42, and [Tyr^{42}]Aβ42 all were relatively shielded from solvent. Analysis of the assembly dependence of the site-specific intrinsic fluorescence data suggests that the CHC is particularly important in controlling Aβ40 assembly, whereas the C-terminus plays the more significant role in Aβ42 assembly.

Amyloid is a generic term describing a macroscopic accretion of proteinaceous fibrils (*1*). These "amyloid fibrils" have a core structure characterized by extended β-sheets in which the β-strands are oriented perpendicular to the fibril axis (cross-β structure) (*2*). In vitro studies have suggested that amyloid fibril formation is a generic property of proteins and many peptides (*3−8*). Amyloid formation is associated with a number of progressive, usually fatal, diseases in humans, including Alzheimer's disease (AD),[1] Parkinson's disease, and the prion diseases (*9, 10*).

In AD, efforts have been made to define the pathway(s) of Aβ fibril assembly. In doing so, an increasing number of intermediates have been discovered, most of which are potent neurotoxins (for recent reviews, see refs *11, 12*). These intermediates include protofibrils (*13−15*), paranuclei (*16*), Aβ-derived diffusible ligands (ADDLs) (*17, 18*), cell-derived oligomers (*19*), and other assemblies (*20, 21*). Detection of ADDLs and other small oligomers in vivo has provided

evidence for the primacy of prefibrillar assemblies in AD neuropathogenesis, a significant paradigm shift in the field (*11, 12, 22−26*).

The implication of a working hypothesis for AD pathogenesis that involves neurotoxic oligomers is that treating the disease requires a detailed understanding of how Aβ monomers fold and oligomerize. Previous in vitro studies of the dynamics of Aβ assembly have used circular dichroism (CD), Fourier transform infrared (FT-IR), and nuclear magnetic resonance (NMR) spectroscopies to monitor conformational (primarily secondary structure) changes during monomer folding and assembly (*13, 27−35*). These studies have shown that RC → β-sheet (*31, 34−36*), α-helix → β-sheet (*30, 32, 33, 36*), and RC → α-helix → β-sheet (*29*) transitions occur. The earliest oligomerization event thus far studied has been pentamer/hexamer (paranucleus) formation by Aβ42 (*16*). CD studies of paranuclei revealed a largely disordered structure, as in monomers. The native structural disorganization of the Aβ monomer, like that of α-synuclein, is termed "natively unfolded" (*37*). Natively unfolded proteins must undergo significant conformational organization during fibril assembly. Experimental studies have suggested that Aβ folding involves formation of a "partially folded" intermediate (*28*). This population of a partially folded conformational space contrasts with the apparent necessity of proteins with native folds to proceed through a "partially unfolded" intermediate state during their pathologic conformational rearrangement into amyloid-forming congeners (for a review, see ref *38*).

* To whom correspondence should be addressed. E-mail: dteplow@
mednet.ucla.edu. Phone: (310) 206-2030. Fax: (310) 206-1700.
‡ David Geffen School of Medicine at UCLA.
§ Boston University.

[1] Abbreviations: Aβ, amyloid β-protein; AD, Alzheimer's disease; Aβ40, Aβ(1−40); Aβ42, Aβ(1−42); LMW, low-molecular weight; FU, arbitrary fluorescence units; PICUP, photoinduced cross-linking of unmodified proteins; CD, circular dichroism spectroscopy; EM, electron microscopy; CHC, central hydrophobic cluster; RC, random coil; NAcTyrA, *N*-acetyl-ʟ-tyrosine amide; SD, standard deviation.

```
Aβ40                DAEFRHDSGYEVHHQKLVFFAEDVGSNKGAIIGLMVGGVV

[Phe10]Aβ40         ---------F------------------------------

[Tyr1 ]Aβ40         Y--------F------------------------------

[Tyr20]Aβ40         ---------F----------Y-------------------

[Tyr30]Aβ40         ---------F--------------------Y---------

[Tyr40]Aβ40         ---------F-----------------------------Y


Aβ42                DAEFRHDSGYEVHHQKLVFFAEDVGSNKGAIIGLMVGGVVIA

[Phe10]Aβ42         ---------F--------------------------------

[Tyr1 ]Aβ42         Y--------F--------------------------------

[Tyr20]Aβ42         ---------F----------Y---------------------

[Tyr30]Aβ42         ---------F--------------------Y-----------

[Tyr42]Aβ42         ---------F-------------------------------Y
```
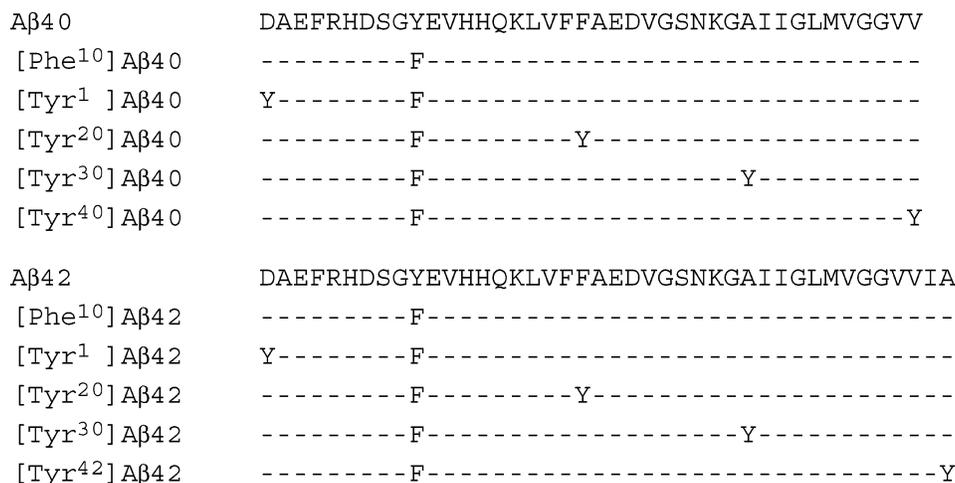
FIGURE 1: Primary structure of Aβ peptides. The name and sequence of each peptide used in our studies are given. Hyphens indicate amino acid residues identical to those in native Aβ. In peptides in which the Tyr probe was placed at positions other than the native position 10, a Phe group was substituted at position 10. For simplicity, these Aβ homologues are specified only by the position of the Tyr ([Tyr^n]). The complete peptide specification would include the positions of both the Tyr and Phe residues (e.g., [Tyr^n,Phe^{10}]).

The next step toward achievement of a full mechanistic understanding of Aβ folding and oligomerization is monitoring these processes using techniques with greater spatial resolution. A powerful approach for site-specific analysis of protein folding utilizes the intrinsic fluorescence of the aromatic amino acids Trp, Tyr, and Phe (*39*). Trp fluoresces strongly, and both the fluorescence intensity and the wavelength at which fluorescence intensity is maximal (λ_{max}) of its indole ring are highly sensitive to solvent polarity and to the presence of fluorescence quenchers. Changes in the immediate vicinity of Trp that occur during protein folding and assembly thus are indicated by alterations in Trp fluorescence. Local environmental changes also alter the fluorescence intensity of Tyr. Solvent exposure decreases Tyr fluorescence without altering the Tyr λ_{max}. In addition, the fluorescence of the Tyr phenol ring can be quenched by exposure to hydrated peptide carbonyl groups and through hydrogen bond formation with peptide carbonyls or with carboxylate side chains of aspartic or glutamic acid (*40, 41*).

Here, we present results of studies of Aβ folding and assembly in which local environmental changes were probed using intrinsic Tyr fluorescence. An advantage of using Tyr as a probe of Aβ structure is that residue 10 in the wild-type peptide is Tyr. Probing the local environment at position 10 thus can be done using the native protein. In addition to studies of wild-type Aβ40 and Aβ42, periodic substitutions of Tyr were introduced from the N-terminus to the C-terminus of each protein. The results reveal site-specific differences in the conformations of monomeric Aβ40 and Aβ42 that may be relevant to alloform-specific folding and assembly.

MATERIALS AND METHODS

Chemicals and Reagents. Chemicals were obtained from Sigma Chemical Co. (St. Louis, MO) and were of the highest purity available. Water was double-distilled and deionized using a Milli-Q system (Millipore Corp., Bedford, MA).

Peptide Synthesis. Aβ peptide synthesis, purification, and characterization were carried out as described previously (*14*). Briefly, Aβ40, Aβ42, their Tyr-substituted peptides (Figure 1), and all pentapeptides (Table 1) were synthesized

Table 1: Pentapeptide Analogues of Aβ[a]

Pentapeptide	Sequence	Intensity ± SD (FU)
[Tyr^1]Aβ(1−5)	H-Tyr-Ala-Glu-Phe-Arg-COOH	8524 ± 400
[Tyr^{10}]Aβ(8−12)	H-Ser-Gly-Tyr-Glu-Val-COOH	7798 ± 535
[Tyr^{20}]Aβ(18−22)	H-Val-Phe-Tyr-Ala-Glu-COOH	10940 ± 636
[Tyr^{30}]Aβ(28−32)	H-Lys-Gly-Tyr-Ile-Ile-COOH	9079 ± 442
[Tyr^{40}]Aβ(38−42)	H-Gly-Val-Tyr-Ile-Ala-COOH	8842 ± 396

[a] Designed peptides, which are homologous with pentapeptide segments of Aβ, were dissolved in 10 mM phosphate buffer (pH 7.4) at 22 °C, at a final peptide concentration of 100−150 µM. Tyr emission spectra of each peptide were acquired immediately using an excitation wavelength of 280 nm and emission measured in the range of 290−500 nm. The maximum fluorescence intensity values at 305 nm were normalized to an arbitrary standard concentration of 140 µM. Results are expressed in average arbitrary fluorescence units (FU) ± SD and are derived from four independent experiments.

on an automated peptide synthesizer (model 433A, Applied Biosystems, Foster City, CA) using 9-fluorenylmethoxycarbonyl-based methods on preloaded Wang resins. Peptides were purified using reversed-phase high-performance liquid chromatography (RP-HPLC). Quantitative amino acid analysis and mass spectrometry yielded the expected compositions and molecular weights, respectively, for each peptide. Selected peptides also were sequenced using automated Edman chemistry (model 477A, Applied Biosystems). Purified peptides were stored as lyophilizates at −20 °C. To maximize chemical homogeneity among related peptides, multiple peptides were synthesized from the same starting resin by resin splitting at sites of sequence variation.

Isolation of Low-Molecular Weight (LMW) Aβ and Its Tyr-Substituted Analogues. Peptide lyophilizates were pretreated with dilute NaOH according to the method of Fezoui et al. (*42*) to increase their solubility and decrease the extent of de novo peptide aggregation. This treatment, and other treatments designed to produce unaggregated "starting" peptide preparations, have not been found to affect the primary structure of the peptide or its subsequent folding and self-assembly (*42−47*). Briefly, peptides were dissolved in 2 mM NaOH at a concentration of ∼1 mg/mL, sonicated for 3 min, and then lyophilized. This treatment was particularly important for Aβ42 and its substituted congeners because of their high propensity to self-associate. The

lyophilizates from NaOH treatment then were dissolved in distilled water and buffered by the addition of 1 volume (v) of double-strength (2×) phosphate buffer (pH 7.4) containing 0.02% (w/v) NaN₃, to yield a final buffer concentration of 10 mM and a final peptide concentration of ∼2 mg/mL (∼0.45 mM). Samples were sonicated for 1 min at 22 °C in an ultrasonic water bath (model B1200-R, Branson Ultrasonics Corp., Danbury, CT), transferred to filters [10000 molecular weight cutoff (MWCO) Centricon YM-10, Millipore Corp.], and centrifuged for 30 min at 16000g using a benchtop microcentrifuge (Eppendorf model 5415C, Brinkmann Instruments Inc., Westbury, NY) (*29*). By definition (*13*), the resulting filtrate is termed low-molecular weight (LMW) Aβ. LMW Aβ has been shown to contain monomeric Aβ in equilibrium with low-order, unstructured oligomers. The concentration of Aβ in the filtrates was determined by quantitative amino acid analysis, as described previously (*48*).

Circular Dichroism Spectroscopy (CD). LMW Aβ samples at concentrations of 50−60 μM were prepared for each CD analysis by gently drawing up, and then expelling, the peptide solution into a 200 μL pipet tip. After three cycles, an aliquot was placed into a 0.1 cm path length quartz cell (Hellma, Forest Hills, NY), and then CD measurements were performed on an Aviv model 62A DS spectropolarimeter (Aviv Associates, Lakewood, NJ). After spectra were recorded, the aliquot was returned to the original sample tube. All measurements were taken at 22 °C. Spectra were generally recorded over the wavelength range of 198−260 nm. Three individual experiments were carried out with each sample. Raw data were manipulated by smoothing and subtraction of buffer spectra, according to the manufacturer's instructions.

Intrinsic Fluorescence. LMW Aβ was incubated at 22 °C at a concentration of 50−60 μM. Samples were prepared for analysis by gently drawing up, and then expelling, the peptide solution into a 200 μL pipet tip. Fluorescence measurements were performed in rectangular 10 mm quartz microcuvettes using a Hitachi F4500 spectrofluorimeter (Hitachi Instruments Inc., Rye, NH) with excitation at 280 nm and emission in the range of 290−500 nm. All fluorescence measurements were carried out at 22 °C with a scan rate of 240 nm/min. Slit widths used for excitation and emission were 5 and 10 nm, respectively. The fluorescence emission spectrum of phosphate buffer (background intensity) was subtracted from the emission spectrum of each peptide sample. The fluorescence intensity of [Phe¹⁰]Aβ40 or [Phe¹⁰]Aβ42 also was subtracted from the spectra of the relevant analogues to ensure that the fluorescence from the sole Tyr residue could be quantified. For DMSO titration experiments, 5 μL aliquots of DMSO were added periodically and directly into a cuvette containing 100 μL of freshly prepared LMW Aβ. Fluorescence measurements were taken immediately after each addition of DMSO. Each resulting spectrum was corrected for any contribution of DMSO by subtracting fluorescence values from appropriate DMSO blanks. Four independent experiments were carried out for each sample. Fluorescence data are expressed in arbitrary fluorescence units (FU).

Fourier Transform Infrared (FTIR) Spectroscopy. FTIR spectra were acquired at 2 cm⁻¹ resolution on a Bruker IFS 66 v/s spectrometer equipped with a liquid nitrogen-cooled HgCdTe detector. Two microliters of Aβ40 (200−250 μM) in 10 mM phosphate buffer in D₂O (pD 7.4) were placed between two 19 mm diameter, 2 mm thick CaF₂ windows separated by a 6 μm Teflon spacer and mounted in a liquid cell (Harrick Scientific Corp., model DLC-M19). The FTIR sample compartment was purged with dry air. Each spectrum consisted of an average of 2500−5000 separate scans. Spectral contributions from water vapor and buffer were interactively subtracted. The raw data were subjected to Fourier self-deconvolution using a resolution enhancement factor of 1.6 and a smoothing factor of 20%. Second-derivative spectra were obtained to determine peak positions following the procedures of Byler and Susi (*49*) and Yang et al. (*50*). Curve fitting within the amide I region (1750−1550 cm⁻¹) of the deconvoluted spectra was accomplished using initial peak positions as determined by the second-derivative spectra (*49*, *50*). All data analysis was performed using the Thermo Galactic Grams/AI 7 software. Three independent experiments were performed.

Electron Microscopy (EM). Five microliters of sample was spotted on a glow-discharged, carbon-coated Formvar grid (Electron Microscopy Sciences, Fort Washington, PA) and incubated for 5 min, washed with distilled water, and then stained with a 1% (w/v) aqueous uranyl formate solution. Uranyl formate solutions were filtered through a 0.2 μm sterile syringe filter (Corning, Acton, MA) before use. EM analysis was performed using a JEOL 1200 transmission electron microscope. Four individual experiments were carried out for each sample.

RESULTS

Experimental and Theoretical Considerations. Both Tyr and Trp are used routinely for intrinsic fluorescence measurements (*39−41*). Because of the relatively small size of Aβ and the absence of strong stabilizing intrapeptide forces in the monomer state, we sought to incorporate a fluorophore-producing maximal fluorescence intensity but possessing minimal size. We chose Tyr because its phenol side chain is less bulky than the indole side chain of Trp, its fluorescence yield [0.14 in water at pH 7 (*51*)] is sufficient to probe Aβ structure, and it exists natively in Aβ at position 10.

Tyr was incorporated at intervals of ∼10 amino acids (positions 1, 10, 20, 30, and 40 or 42) into Aβ40 and Aβ42 (Figure 1). Aβ contains four aromatic amino acids. The three Phe residues, Phe⁴, Phe¹⁹, and Phe²⁰, are fluorometrically silent because of their low quantum yield (*51*). Tyr¹⁰ provides a probe of native structure in the N-terminal region. However, the presence of Tyr¹⁰ in peptides containing Tyr at additional sites would complicate the interpretation of the resulting fluorescence data. For this reason, Tyr¹⁰ was replaced with Phe in the other substituted Aβ peptides. This conservative substitution produced a structural difference at position 10 consisting solely of the loss of the *p*-hydroxyl group from the phenolic ring of Tyr. Statistical studies of naturally occurring amino acid substitutions in proteins show that the replacement of Tyr with Phe is the only replacement with a favorable probability of occurrence (*52*).

Experimental evidence also suggests that Tyr substitutions should allow normal peptide folding and assembly. Analysis of Aβ N-terminal structure within peptide monomers and fibrils suggests relative disorder in this region (*53*, *54*). Thus,
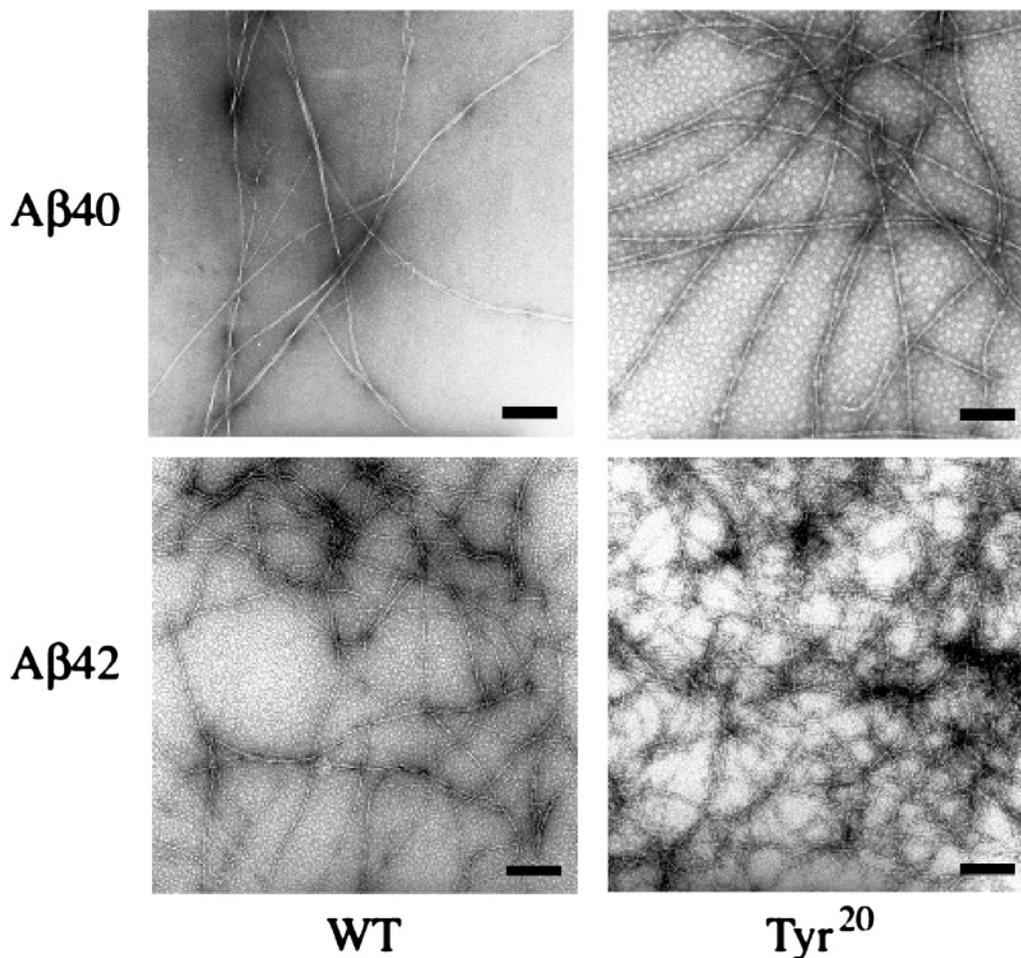
FIGURE 2: Morphology of Aβ assemblies. Aliquots were removed from peptide assembly reaction mixtures at their completion and spotted on glow-discharged, carbon-coated Formvar grids. Transmission electron microscopy (TEM) then was performed after negative staining. Micrographs of Aβ40, [Tyr[20]]Aβ40, Aβ42, and [Tyr[20]]Aβ42 are shown. These are representative of the morphologies observed for the 10 different Aβ peptides that were studied. Scale bars are 100 nm.

the Asp[1] → Tyr substitution would not be expected to cause significant changes in the biophysical properties of Aβ. At positions 30, 40, and 42, Tyr replaces the aliphatic groups Ala, Val, and Ala, respectively. Substitution of Val[40] with Trp has been used previously and successfully to study Aβ C-terminal structure (*55*). Tyr substitution at position 40 would be less likely to produce spurious results. By analogy, the Tyr[42] substitution in Aβ42 also should produce normal peptide folding and assembly. We note that Török et al. (*56*) have synthesized a series of 19 Aβ peptides, each containing the 1-oxyl-2,2,5,5-tetramethyl-D-pyrroline-3-methylcystinyl spin-label at a different position. This spin-label is substantially larger than Tyr. The spin-labeled peptides all assembled into fibrils that were morphologically indistinguishable from fibrils formed by unsubstituted Aβ peptides. Of relevance to the probe strategy here is the fact that these peptides included substitutions at positions 10, 20, 29, 32, 40, and 42. In silico studies of the folding and oligomerization of Aβ(10−35), Aβ40, and Aβ42 all reveal extensive hydrophobic interactions among amino acids in the C-terminal portion of Aβ (*57, 58*). Tyr substitution for Ala[30], Val[40], and Ala[42] would not be expected to significantly affect this type of interaction.

To compare secondary structure dynamics among the native and substituted peptides, CD experiments were performed on peptide solutions immediately after their preparation and during their assembly (data not shown). All peptides were predominantly disordered initially, but then displayed characteristic RC → α-helix → β-sheet transitions during oligomerization and fibril formation, as reported previously (*29*). These data support our argument that the Aβ peptides containing Tyr substitutions fold in a manner indistinguishable from that of the parent peptides.

Morphologic Analysis of Aβ Assemblies. Electron microscopy was used to determine the morphologies of the end-stage assemblies formed by the wild-type and Tyr-substituted peptides. All 10 peptides formed amyloid-like fibrils that typically displayed a helical ultrastructure and varying degrees of lateral association. The fibrils were composed of one or more filaments, resulting in overall diameters ranging from ∼4 to 12 nm. Representative data are shown in Figure 2. Aβ40 formed helically wound fibrils of indeterminate length with diameters of ∼8 nm. [Tyr[20]]Aβ40 formed fibrils with a similar morphology. Aβ42 produced both long and short fibrils that often were narrower (∼4−5 nm) than fibrils seen in Aβ40 samples. Like Aβ42, [Tyr[20]]Aβ42 formed long fibrils with diameters of ∼4 nm. The fibril morphologies observed for the other Aβ40 and Aβ42 analogues (data not shown) were similar to those formed by each respective wild-type peptide. These data show that Tyr substitution in Aβ40 or Aβ42 did not cause significant perturbations in amyloid fibril assembly.

Temporal Changes in the Intrinsic Fluorescence during Aβ Assembly. To study site-specific environmental characteristics of Aβ during peptide folding and self-assembly, Tyr fluorescence was monitored (Figure 3A,B). To do so, Aβ samples were prepared at concentrations of 50−60 μM in 10 mM phosphate buffer (pH 7.4) and then incubated at 22 °C without agitation. The fluorescence intensity of mono-tyrosinated Aβ in the concentration range 50−60 μM is substantial (10000 FU), allowing facile monitoring of conformational changes during peptide self-assembly. Significant differences in fluorescence intensity were observed immediately after the initiation of the experiments (Figure 3A,B). Aβ40 (Tyr[10]) and the Tyr[1] analogue had equivalent intensities of ~4000 FU. The Tyr[20] and Tyr[30] analogues had intensities of ~6000 and ~11000 FU, respectively. [Tyr[40]]Aβ40 displayed the highest initial intensity, ~20000 FU. During assembly, Aβ40, [Tyr[1]]Aβ40, [Tyr[30]]Aβ40, and [Tyr[40]]Aβ40 all displayed modest monotonic decreases in fluorescence intensity (Figure 3A). In contrast, an increase in intensity was seen with [Tyr[20]]Aβ40. Correlation of these data with CD experiments (data not shown) showed that the initial phase (prior to day 6) of the increase coincided with the RC → α-helix transition linked to formation of an oligomeric, α-helix-rich intermediate (*29*). The exponential increase in fluorescence intensity coincided with the subsequent α-helix → β-sheet transition associated with fibril formation (*29*).

The Aβ42 peptide series, like that of Aβ40, displayed peptide-specific differences in initial intensity (Figure 3B). Aβ42, [Tyr[1]]Aβ42, and [Tyr[20]]Aβ42 had very similar intensities, all of which were 2−3-fold lower than those of [Tyr[30]]Aβ42 and [Tyr[42]]Aβ42. [Tyr[30]]Aβ42 had the highest intensity of any peptide in either series, ~28000 FU. With the exception of the wild-type peptides and the C-terminally labeled peptides [Tyr[40]]Aβ40 and [Tyr[42]]Aβ42, which produced similar initial intensities, all of the Aβ42 peptides fluoresced with intensities 2−2.5-fold higher than those of the Aβ40 series (Figure 4). The intensity of [Tyr[42]]Aβ42 fluorescence was modestly higher than that of [Tyr[40]]Aβ40 (~23000 vs ~20000 FU, respectively). All Aβ42 peptides displayed maximal fluorescence immediately upon incubation (Figure 3B). Thereafter, the fluorescence intensity decreased monotonically. The sigmoidal increase in fluorescence intensity observed with [Tyr[20]]Aβ40 was not seen with [Tyr[20]]Aβ42. The Aβ42 peptides did exhibit a temporal decrease in fluorescence intensity similar to that of the Aβ40 peptides, but with an accelerated kinetics.

Role of Amino Acid Sequence in Fluorescence Intensity. The fluorescence intensity differences observed in the Aβ42 peptides versus the Aβ40 peptides were intriguing. If the initial conformational state of the peptides was that of a relatively disordered monomer, then the fluorescence intensity of a probe should depend primarily on the sequence of the peptide segment within which the probe was inserted. The sequences of Aβ40 and Aβ42 are identical through Val[40]; therefore, it would be reasonable to predict that the fluorescence intensities of the [Tyr[1]]Aβ40 and [Tyr[1]]Aβ42 peptide pair also should be identical. Similarly, the fluorescence of each member of the Tyr[10], Tyr[20], and Tyr[30] pairs should be identical, although intensities among pairs might vary. As shown in Figure 4, both significant intrapair and interpair differences in fluorescence intensity were observed. A logical explanation for the failure of the aforementioned
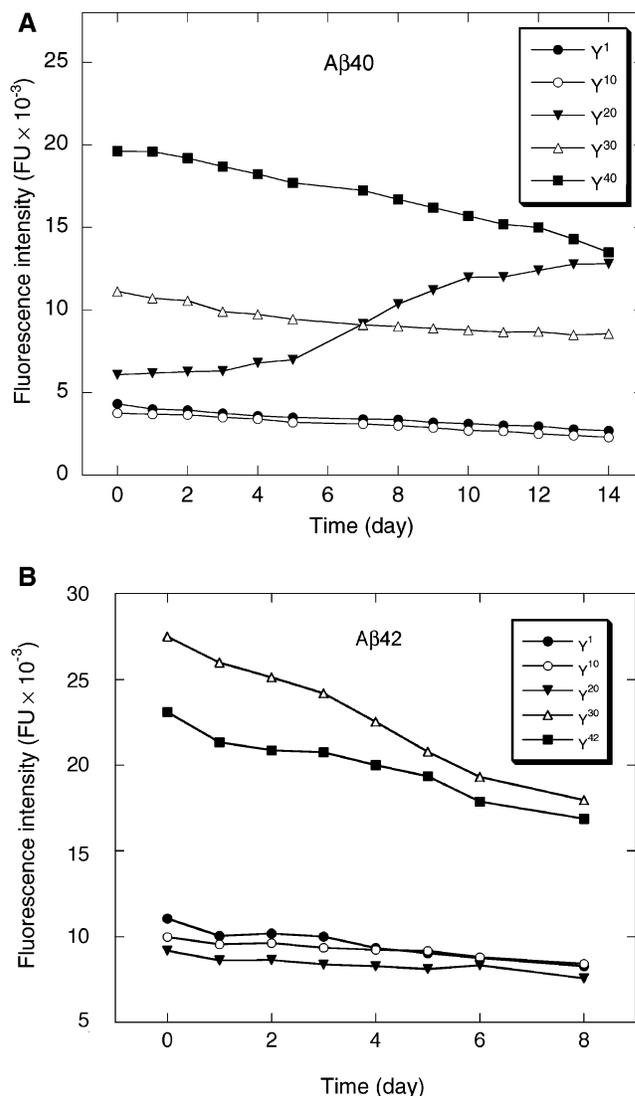

FIGURE 3: Intrinsic Tyr fluorescence. (A) LMW Aβ40 and its Tyr-substituted analogues were incubated at a concentration of 50−60 μM in 10 mM phosphate (pH 7.4) at 22 °C. Tyr emission spectra were acquired daily for 14 days. The maximum intensity at 305 nm is plotted against time (days). Each spectrum was normalized to a concentration of 60 μM. Results are expressed in arbitrary fluorescence units (FU) and are representative of those obtained in each of four independent experiments. (B) Aβ42 and its Tyr-substituted analogues. Spectra were acquired as described above. Monitoring ended after 8 days, at which time fibrils had formed.

prediction is that the Aβ40 and Aβ42 peptide families differ structurally.

To formally examine the question of the sequence dependence of the fluorescence intensity, we designed and synthesized five pentapeptides, each of which corresponded to a site of Tyr substitution. The fluorescence intensities for these peptides then were determined (Table 1). The average fluorescence intensity $I \pm$ SD was 9037 ± 1168, which produced a relative standard deviation (RSD = SD/average intensity) of ≈13%. [Tyr[20]]Aβ(18−22) was most fluorescent, likely due to sensitized fluorescence arising from energy transfer from the neighboring Phe[19] (*59*). Elimination of Tyr[20] from the statistical analysis produced a slightly lower average intensity, 8561 ± 557, and halved the RSD to ~6%. The magnitude of the RSD demonstrates that little sequence-specific variation in fluorescence intensity occurs. This
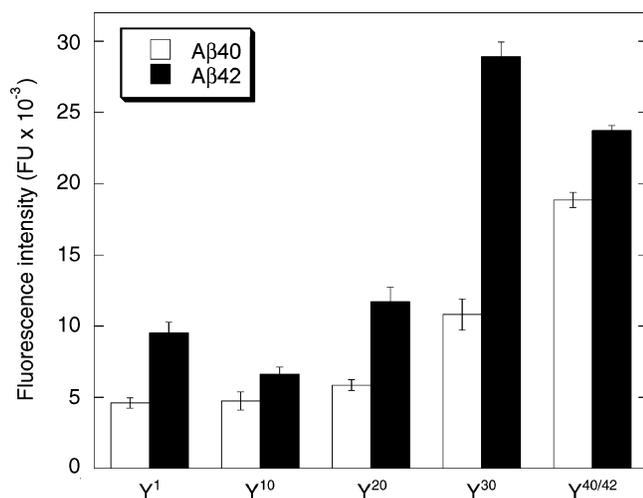
FIGURE 4: Initial fluorescence intensities of Aβ40 peptides (white bars) and Aβ42 peptides (black bars). The initial maximum fluorescence intensity at 305 nm (at day 0) of all peptides was normalized to a concentration of 60 μM. Results are expressed in arbitrary fluorescence units (FU) and are representative of those obtained in each of four independent experiments.

statistical analysis, and visual inspection of the data in Table 1, show that the magnitude of the observed fluorescence differences among members of the Aβ40 and Aβ42 families cannot be explained on the basis of sequence-specific effects. Rather, the differences must result from conformational differences among the peptides.

Solvent Exposure of Fluorogenic Groups. It has been suggested that the excited singlet states of Trp or Tyr interact with neighboring water molecules to form excited state–water complexes (exciplexes) and that such complexation competes with the radiative decay of the fluorophore excited state (*60−62*). The result is a diminution in fluorescence yield. However, if organic solvents (e.g., DMSO or dioxane) are added to the aqueous milieu in which fluorescence experiments are conducted, an enhancement of fluorescence can be achieved. The enhancement of fluorescence associated with organic cosolvents is thought to result from the decreased concentration of water in the immediate vicinity of the fluorophore and the consequent reduction in the level of exciplex formation (*60−62*). Decreased carbonyl group hydration also can produce an effective increase in Tyr fluorescence because hydrated peptide carbonyl groups quench Tyr fluorescence (*40*). Mixed solvent systems thus can provide information about the microenvironment of the excited-state fluorophore. In solvent-protected structures, e.g., in the core of a globular protein, changes in solvent composition that do not denature the protein do not affect the microenvironment of Tyr and therefore do not produce differences in fluorescence intensity. In contrast, if Tyr is solvent-exposed, significant solvent dependency of the fluorescence intensity is observed. Solvent perturbation of spectroscopic properties of amino acids has been used frequently to assess amino acid exposure in proteins (*63−65*).

To evaluate site-specific solvent exposure of the Tyr fluor, we used a DMSO/water mixed-solvent system. We first established the behavior of the tyrosine fluor by studying the fluorescence characteristics of *N*-acetyl-L-tyrosine amide (NAcTyrA), a proxy for tyrosine within fully denatured

Table 2: Solvent Effects on Tyr Fluorescence[a]

Compound	Solvent	Intensity ± SD (FU)
Tyr	buffer	8274 ± 120
NAcTyrA	buffer	5110 ± 200
NAcTyrA	water	5206 ± 212
NAcTyrA	DMSO	9757 ± 412

[a] Fluorescence measurements of Tyr and NAcTyrA were made in distilled water and 10 mM phosphate buffer (pH 7.4) containing 0.01% (w/v) sodium azide, and in DMSO. Amino acid concentrations ranged from 20 to 30 μM. Excitation was done at 280 nm, and emission was monitored in the range of 290−500 nm. Results are expressed in arbitrary fluorescence units (FU) ± SD. The λ_{max} for emission was 306 ± 2 nm. Fluorescence intensities at this wavelength were normalized to an amino acid concentration of 60 μM. These results are representative of those obtained in each of four independent experiments.

proteins. Because phosphate ions, at sufficient concentration, are effective quenchers of Tyr fluorescence (*41*), we determined the fluorescence intensity of NAcTyrA in the 10 mM phosphate buffer used in our assembly experiments. For comparison, fluorescence experiments on the free Tyr amino acid also were performed. The fluorescence of NAcTyrA in buffered and unbuffered water was similar, ∼5000 FU (Table 2), indicating that the buffer used in our experiments did not quench the fluorescence. The fluorescence of the free Tyr amino acid was ∼60% higher than that of NAcTyrA (Table 2), suggesting that amide groups in NAcTyrA quenched Tyr fluorescence. When the solvent was changed from water to DMSO, the corrected (see Materials and Methods) fluorescence intensity of NAcTyrA approximately doubled (Table 2). In water, the emission maximum, λ_{max}, of Tyr and NAcTyrA was ∼304 nm (data not shown). Changes in solvent polarity, associated with the use of water or DMSO, did not change λ_{max} significantly [$\Delta\lambda_{max} \approx 3-4$ nm (data not shown)].

We next determined the concentration dependence of the DMSO enhancement of fluorescence. To do so, 5 μL aliquots of DMSO were added successively to a cuvette containing 100 μL of 20 μM Tyr or NAcTyrA. Fluorescence measurements were taken immediately after each addition. The fluorescence intensities of NAcTyrA and free Tyr increased monotonically with an increase in DMSO concentration (Figure 5). Linear regression analysis of the data revealed that the DMSO concentration dependence of the fluorescence of NAcTyrA, as quantified by the slope of the dependence line, was 9.3-fold greater than that displayed by free Tyr. This suggests that in addition to decreasing fluorescence quenching by water, DMSO relieved quenching produced by the amide groups of NAcTyrA.

Cosolvent studies of the Aβ40 and Aβ42 series peptides then were performed to determine whether solvent-dependent quenching of the peptides explained the prior observed differences in fluorescence intensity. Figure 6A shows the DMSO concentration dependence of the Aβ40 series peptide fluorescence intensity. A monotonic increase in Tyr fluorescence intensity was observed for all peptides. The quasi-linear nature of the increase indicates that the change in fluorescence intensity likely is due to interaction of Tyr with solvent and not to major structural changes in the peptide backbone. NAcTyrA displayed a fluorescence intensity increase of 80% across the DMSO concentration range (0−23%). Aβ40, [Tyr[1]]Aβ40, [Tyr[20]]Aβ40, and [Tyr[30]]Aβ40
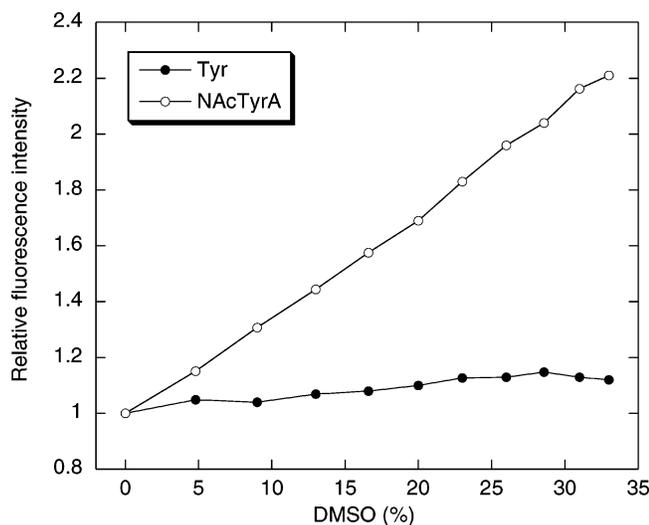
FIGURE 5: Fluorescence intensity of NAcTyrA and free Tyr. Fluorescence spectra of NAcTyrA (O) and Tyr (●) were acquired during iterative addition of DMSO. The data were corrected for contributions of DMSO itself to the fluorescence intensity and for alterations in volume produced by DMSO addition. Relative fluorescence intensities (FU) at 305 nm are plotted against DMSO percentage (v/v). The difference in the slopes between Tyr and NAcTyrA was statistically significant ($p < 0.003$), as determined using the Student's *t*-test (SigmaPlot 7.0, SPSS Inc., Chicago, IL).

displayed an ∼60% increase, indicating that Tyr in these peptides is exposed to solvent, but not as fully as is NAcTyrA. The fluorescence intensity of [Tyr[40]]Aβ40 increased about half as much (∼30%) as did that of the other peptides in the Aβ40 series, suggesting that the C-terminus of Aβ40 is more shielded from solvent than are the more N-terminal regions. Intra- or intermolecular structure formation may account for this. For example, Aβ oligomerization is known to occur concurrently with preparation of LMW Aβ (*16*). This possibility is consistent with the observation that Trp[40] is solvent shielded in [Trp[40]]Aβ40 dimers (*55*).

Cosolvent titrations of Aβ42 and its Tyr-substituted analogues produced data qualitatively similar to those of the Aβ40 series. All peptides displayed monotonic, DMSO concentration-dependent increases in fluorescence intensity (Figure 6B). At the highest DMSO concentration, 23%, the fluorescence intensity of Aβ42, [Tyr[1]]Aβ42, and [Tyr[20]]Aβ42 was ∼40% higher than that observed in the absence of DMSO. The magnitude of the increase in intensity was smallest (∼5%) for [Tyr[42]]Aβ42. The Aβ40 homologue, [Tyr[40]]Aβ40, also produced the smallest increase among its family members. The most obvious difference between the two Aβ families was the behavior of [Tyr[30]]Aβ42. Its intensity increase, ∼10%, was substantially smaller than the increase seen for the peptides in which Tyr substitutions were made more N-terminally, making its behavior more like that of [Tyr[42]]Aβ42. The decreased magnitude of the DMSO-induced fluorescence intensity increase in the Aβ42 peptide series, relative to that of the Aβ40 peptide series, suggests that each of the respective Tyr residues in Aβ42 is less solvent-exposed than their homologues in the Aβ40 series. For both series, C-terminal Tyr groups (Tyr[40] and Tyr[42]) are least exposed, suggesting that the C-terminus is sequestered through intramolecular folding or intermolecular interactions, e.g., oligomer formation.
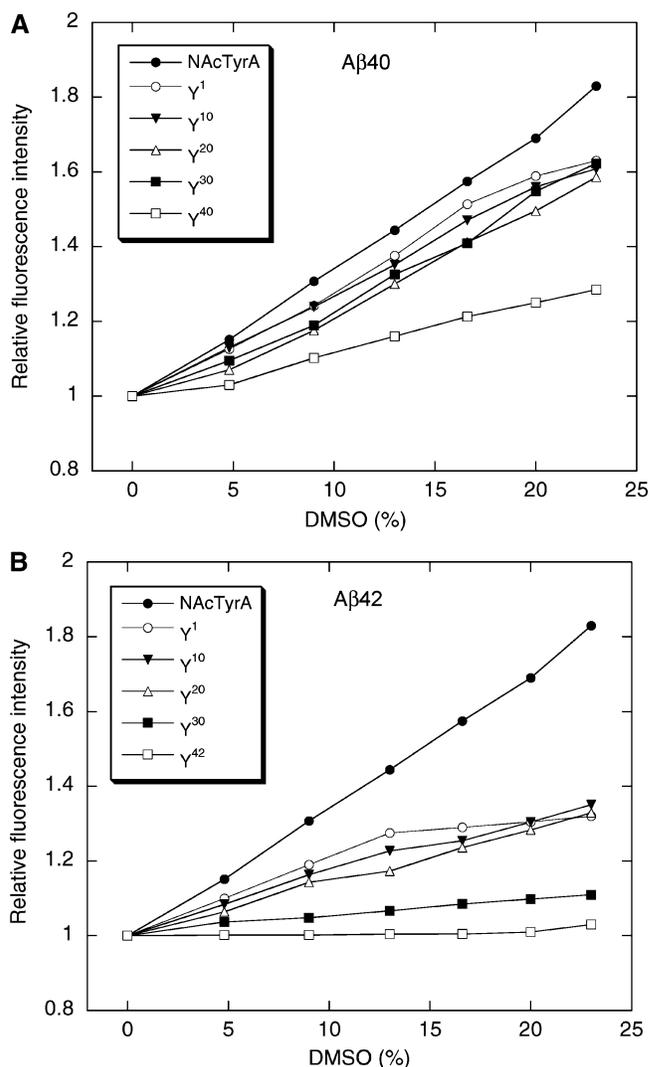

FIGURE 6: Effects of cosolvent on intrinsic fluorescence. Fluorescence spectra of LMW Aβ were acquired in the presence of increasing amounts of DMSO (0−23%, v/v). Peptides were prepared at a concentration of 50−60 μM in 10 mM phosphate (pH 7.4) at 22 °C. Contributions of DMSO to the fluorescence intensity, and alterations in volume due to DMSO addition, were controlled as detailed in the legend of Figure 5. The relative fluorescence intensity (FU) at 305 nm is plotted against DMSO percentage (v/v): (A) Aβ40 and analogues and (B) Aβ42 and analogues.

Solvent Effects on Aβ Conformation. To investigate the possibility that DMSO-associated changes in fluorescence were due to solvent-induced secondary structure changes in Aβ and not fluorophore−solvent interactions, LMW Aβ40 was analyzed by FTIR spectroscopy in the presence and absence of 20% (v/v) DMSO. DMSO does not absorb significant quantities of light in the amide I region (1600−1700 cm^{-1}) of the infrared spectrum (data not shown), enabling the use of FTIR in determining the secondary structure of proteins and peptides in the presence of DMSO (*66, 67*). In contrast, the strong absorbance of DMSO in the ultraviolet wavelength range precludes the use of CD. FTIR experiments were conducted using Aβ40 at a concentration of 200−250 μM in 10 mM phosphate buffer in D$_2$O (pD 7.4) (see Materials and Methods). Curve fitting of the Fourier self-deconvolved spectra using second-derivative spectra to establish peak positions revealed three major bands, at
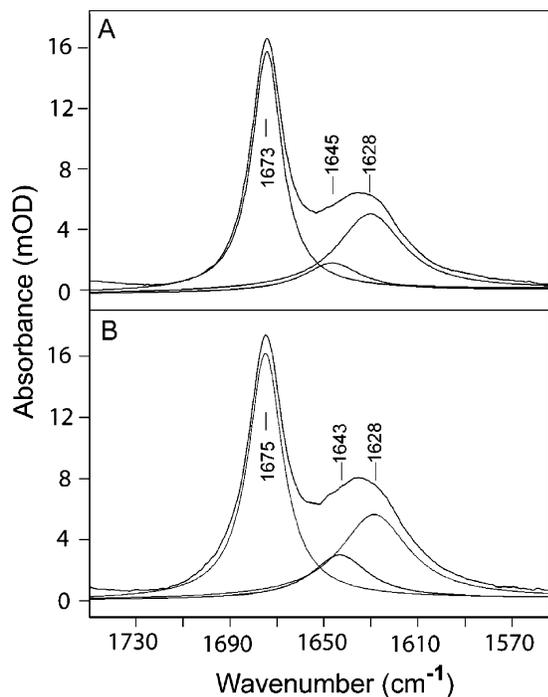
FIGURE 7: Secondary structure of Aβ40. FTIR spectroscopy of Aβ40 was performed in the presence (A) and absence (B) of 20% (v/v) DMSO. Absorbance (mOD) is plotted versus wavenumber (cm⁻¹). The uppermost curve in each panel is the undeconvolved spectrum, from which three components were derived by curve fitting using Lorentzian functions starting with a full width at half-maximum (fwhm) value of 10 cm⁻¹ and peak frequencies determined using Fourier self-deconvolution and second-derivative spectra (see Materials and Methods). The nodes of each of the deconvolved spectra are noted by tick marks and specified by wavenumber.

~1674, ~1644, and ~1628 cm⁻¹ (Figure 7). In the presence of DMSO (Figure 7A), these bands represented 53, 36, and 11%, respectively, of the total amide I absorbance (determined by integrating the area under each band). In the absence of 20% DMSO (Figure 7B), the relative percentages of each band were 53, 32, and 15, respectively, values similar to those obtained with DMSO. The intense band at 1674 cm⁻¹ is produced by residual trifluoroacetate counterion arising from chemical synthesis of Aβ (*68*). The bands at 1644 and 1628 cm⁻¹ were assigned as random coil and β-sheet conformation, respectively (*49, 66*). The 1644 cm⁻¹ band is unlikely to come from water as there is no band in the 1640 cm⁻¹ region in the solvent spectrum. Taken together, these data show that the conformation of Aβ40 does not change significantly in the presence of 20% DMSO.

Experiments with Aβ42 were not possible because of rapid aggregation of the peptide at the concentrations required for FTIR (~200–300 µM). We infer from the FTIR data on Aβ40 that DMSO-induced conformational changes in Aβ42 are unlikely under similar conditions. This inference is consistent with comparative experimental and theoretical work on Aβ40 and Aβ42 that suggests that Aβ42 is intrinsically more stable than Aβ40 and thus is less likely to be affected by low concentrations of DMSO (*16, 54, 57*). In the context of our experiments, "stable" refers to the free energy differences between the conformational states found in aqueous or mixed-solvent systems. Results of studies of the structure, folding, and assembly dynamics of Aβ conducted using NMR (*54*), chemical cross-linking (*16, 69*),

CD (*28*), AFM (*18*), and discrete molecular dynamics simulations (*57*) all are consistent with the postulation that any DMSO-induced conformational transitions of Aβ42 would occur at DMSO concentrations higher than those producing equivalent changes in Aβ40.

DISCUSSION

Recognition of the importance of Aβ oligomers in AD pathogenesis has provided new urgency to understanding early phases of peptide self-association (*11, 12, 26, 70*). Elucidating the assembly-dependent conformational dynamics of Aβ monomers during fibril assembly has been difficult because of the relatively high concentration dependencies of the fibril formation process. Monomers have been produced and studied at nanomolar concentrations (*47*) using immunological methods, but oligomerization events leading to fibril assembly do not occur in these concentration regimes. Here, we used intrinsic fluorescence to probe site-specific conformational changes during assembly of LMW Aβ40 and Aβ42 into fibrils. Data obtained immediately upon preparation of these peptides are relevant to the monomer and low-order oligomer state, as LMW Aβ40 has been shown to comprise an equilibrium mixture predominately of monomers, dimers, trimers, and tetramers and Aβ42 has been shown to comprise a mixture of monomers and oligomers (as large as hexamers or heptamers) (*16, 71*). Data obtained coincident with α-helix formation correlate structurally with oligomers exceeding 100 000 in molecular weight (*29*). As α-helix → β-sheet transitions occur, protofibrils and fibrils are observed (*13, 14*).

We observed differences between Aβ40 and Aβ42 involving solvent accessibility and conformation. The fact that Aβ40 and Aβ42 have identical primary structure, through and including Val⁴⁰, allowed inferences to be made about peptide tertiary and quaternary structure differences, free of potential confounding sequence-specific effects. Thus, pairwise comparison of homologous substituted peptides showed that Aβ42 fluorescence was consistently higher than that of Aβ40. This suggests that Aβ42 is globally more solvent-protected than is Aβ40, an indication that Aβ42 is intrinsically more structured than Aβ40. Cosolvent experiments, in which fluorescence was measured in the presence of increasing concentrations of DMSO, showed that the C-termini of Aβ40 and Aβ42 both were more structured than their corresponding N-termini. Relevant to these observations are recent in silico studies of Aβ oligomerization that show a high probability of Val⁴⁰ forming numerous intramolecular contacts with apolar residues (*57*). These interactions would be expected to have two consequences: (1) partial protection from solvent quenching and (2) less quenching from polar side chains or hydrated amide bonds. This could explain why [Tyr⁴⁰]Aβ40 displayed the highest absolute fluorescence in the absence of DMSO. The higher absolute fluorescence intensity of [Tyr³⁰]Aβ40, relative to those of Aβ40, [Tyr¹]Aβ40, and [Tyr²⁰]Aβ40 (Figure 3A), may result from similar factors. In the more polar N-terminal portion of Aβ, within which the Tyr probe was located in the latter three peptides, both solvent- and peptide-mediated quenching could occur simultaneously, accounting for the lower fluorescence intensities observed in these peptides. If so, these peptides would be predicted to be more sensitive to cosolvent-

mediated diminution of quenching—a result observed experimentally.

For Aβ42, simulations of oligomerization have shown that the Ile[41]-Ala[42] dipeptide increases the number of intramolecular hydrophobic interactions among C-terminal residues, leading to conformational stabilization (*57*). Additional experimental studies provide evidence of the contribution of the Ile[41]-Ala[42] dipeptide in structural stabilization. For example, Aβ42, but not Aβ40, forms discrete, quasi-globular oligomeric structures, including paranuclei (*16*) and Aβ-derived diffusible ligands (ADDLs) (*17, 18*). Although a well-defined fold for these oligomeric assemblies, akin to those of larger, stable globular proteins, has not been defined, the oligomer size distributions of paranuclei and ADDLs are discontinuous, displaying nodes at pentamer/hexamer, dodecamer, octadecamer, etc. This suggests that the larger assemblies comprise various numbers of a basic structural unit. To form these structural units, the component peptides must have at least partial order. Solution NMR studies of monomeric [Met(O)[35]]Aβ40 and [Met(O)[35]]Aβ42 have shown that the C-terminus of Aβ42 (Gly[29]−Ala[42]) is less flexible, and thus more structured, than the C-terminus of Aβ40 (*54*). Hou et al. recently measured $^1H_\alpha$, $^{13}C_\alpha$, and $^{13}C_\beta$ chemical shift indices of Aβ40, Aβ42, [Met(O)[35]]Aβ40, and [Met(O)[35]]Aβ42 and found that the C-terminus of Aβ42 has a tendency to form β-sheet structure, whereas that of Aβ40 does not (*72*). Considered together with the results of our fluorescence experiments, the data suggest that the C-terminal region is a primary force driving self-association of Aβ42.

The most prominent local structural difference between Aβ40 and Aβ42 was in the CHC. Here, a significant structural rearrangement occurred during Aβ40 assembly that was not observed during Aβ42 assembly. Of the 10 full-length peptides we studied, [Tyr[20]]Aβ40 was the only one that did not display a monotonic, assembly-dependent decrease in fluorescence intensity (Figure 3). This result bears on the relative importance of the CHC and the C-terminus in assembly of Aβ40 and Aβ42, respectively. Structural changes in the CHC can alter Aβ self-assembly significantly. For example, Wood et al. used scanning Pro mutagenesis to demonstrate that Pro substitutions within and adjacent to the CHC (Leu[17]−Asp[23]) prevent fibril formation (*73*). Studies of fibril nucleation and elongation conducted using quasi-elastic light scattering spectroscopy showed that a Pro[19] substitution blocked fibril nucleation (*74*). Zhang et al. have suggested that the initial conformation of the Aβ monomer is a "collapsed coil" in which the CHC forms an unusual folded structure (*75*). Although Tyr[20] exists within a strongly hydrophobic peptide segment (Leu[17]−Ala[21]) in which polar quenching groups are absent, hydrogen bonding between the phenolic hydroxyl group of Tyr and peptide bond carbonyl groups, or interactions between the Tyr side chain and those of neighboring Glu[22] or Asp[23] residues, can strongly quench Tyr fluorescence (*41*). This type of interaction may occur within the collapsed coil structure of the CHC. During peptide self-assembly, the fluorescence intensity of [Tyr[20]]-Aβ40 initially increased slowly, but at ∼5 days an upward inflection was observed, after which the intensity increased rapidly (Figure 3A). This rapid increase at 6−8 days coincides with the conversion of an oligomeric, α-helix-containing intermediate into amyloid fibrils (*29*). After assembly is complete (∼14 days), the fluorescence intensity

increase exceeds 100%. This suggests that assembly of Aβ40 involves substantial structural rearrangement of a folded CHC region. The data are consistent with the interpretation that the CHC "fold" may be helical and that the quenching observed in this conformer comes from intramolecular side chain−backbone interaction or intermolecular helix−helix interactions. Studies of the temperature dependence of Aβ40 fibril elongation also have suggested that conformational rearrangement of Aβ occurs during monomer addition at the fibril tip (*76*). Structural rearrangement was not apparent from analysis of the data from [Tyr[20]]Aβ42 assembly, which showed a gradually decreasing fluorescence intensity during aggregation (Figure 3B).

The end result of amyloidogenic assembly of Aβ40 and Aβ42 is fibrils. However, the pathways to this state followed by Aβ40 and Aβ42 may differ, and these differences may include the formation of intermediates with distinct morphologies and biologic properties. The fluorescence data presented here are consistent with the supposition that the CHC affects Aβ40 assembly particularly strongly and the C-terminus affects Aβ42 assembly particularly strongly. Our fluorescence data also suggest that side chain carboxylates of Glu[22] and Asp[23] may be involved in the initial structural organization of the CHC of unassembled Aβ40. This conclusion is consistent with experimental (*77*) and computational (*78*) studies of Aβ monomer structure. Studies of the effects of amino acid substitutions associated with familial forms of AD (FAD) and cerebral amyloid angiopathy (CAA) also support this idea. These latter studies emphasize the fact that primary structure differences may alter the relative contributions of the CHC, C-terminus, and N-terminus toward control of peptide assembly. For example, Bitan et al. synthesized Aβ40 and Aβ42 peptides containing the FAD/CAA-linked substitutions Ala[21] → Gly, Glu[22] → Gly, Glu[22] → Lys, Glu[22] → Gln, and Asp[23] → Asn, and the non-natural substitution Phe[19] → Pro. Characterization of the oligomer size distributions of LMW preparations of these peptides revealed that naturally occurring substitutions of residues 22 and 23 in Aβ40 produced distributions containing amounts of high-order oligomers greater than that produced by wild-type Aβ40. In addition, the gel mobility of the high-order oligomers formed by the Glu[22] homologues was higher than that of the wild-type oligomers, suggesting that the oligomers had structures more compact than those formed by wild-type peptides. These effects were not observed in similar experiments conducted with Aβ42 (*69*). Glu[22] and Asp[23] in Aβ40 also affected assembly-dependent conformational transitions, whereas these effects were not prominent with Aβ42 (*29*). Specifically, the Glu[22] → Gly and Glu[22] → Gln substitutions significantly accelerated the kinetics of formation of an α-helix-rich intermediate, whereas equivalent effects were not seen in studies of Aβ42 (*29*).

Placement of the Tyr probe in Aβ within the C-terminal region (position 30 or 40/42) revealed a significant assembly-dependent decrease in the fluorescence (Figure 3). Previous studies of Aβ fibril formation have suggested that a turn forms in the peptide segment of residues 22−30 (*53, 79*). In addition, the fibril model derived from solid-state NMR data includes a salt bridge between Asp[23] and Lys[28] (*53*). The formation of a turn structure stabilized in part by a salt bridge would produce significant local environmental changes at residue 30 that would be reflected in assembly-dependent

alterations in fluorescence quenching. This type of alteration was observed for $A\beta 40$ and $A\beta 42$. A second feature of fibril models is the stacking of $A\beta$ monomers through intermolecular hydrogen bonding and side chain packing. In parallel β-sheet models, this juxtaposes the C-termini of $A\beta$ monomers within the hydrophobic core of the amyloid fibril (*53, 80*). In hydrophobic environments, carboxylate anion is a highly effective quencher of Tyr fluorescence. Intermolecular interactions between the Tyr hydroxyl and C-terminal carboxylate ion may be responsible for the gradual decrease in Tyr[40] and Tyr[42] fluorescence observed in our experiments (Figure 3).

ACKNOWLEDGMENT

REFERENCES

1. Virchow, R. (1854) Ueber eine im Gehirn und Rückenmark des Menschen aufgefundene Substanz mit der chemsichen Reaction der Cellulose [On a new substance found in the human brain and spinal cord which reacts chemically like cellulose], *Virchows Arch. Pathol. Anat. Physiol. 6*, 135−137.

2. Kirschner, D. A., Abraham, C., and Selkoe, D. J. (1986) X-ray diffraction from intraneuronal paired helical filaments and extraneuronal amyloid fibers in Alzheimer's disease indicates cross-β conformation, *Proc. Natl. Acad. Sci. U.S.A. 83*, 503−507.

3. Dobson, C. M. (1999) Protein misfolding, evolution and disease, *Trends Biochem. Sci. 24*, 329−332.

4. Guijarro, J. I., Sunde, M., Jones, J. A., Campbell, I. D., and Dobson, C. M. (1998) Amyloid fibril formation by an SH3 domain, *Proc. Natl. Acad. Sci. U.S.A. 95*, 4224−4228.

5. Chiti, F., Webster, P., Taddei, N., Clark, A., Stefani, M., Ramponi, G., and Dobson, C. M. (1999) Designing conditions for *in vitro* formation of amyloid protofilaments and fibrils, *Proc. Natl. Acad. Sci. U.S.A. 96*, 3590−3594.

6. Fezoui, Y., Hartley, D. M., Walsh, D. M., Selkoe, D. J., Osterhout, J. J., and Teplow, D. B. (2000) A *de novo* designed helix-turn-helix peptide forms nontoxic amyloid fibrils, *Nat. Struct. Biol. 7*, 1095−1099.

7. West, M. W., Wang, W. X., Patterson, J., Mancias, J. D., Beasley, J. R., and Hecht, M. H. (1999) *De novo* amyloid proteins from designed combinatorial libraries, *Proc. Natl. Acad. Sci. U.S.A. 96*, 11211−11216.

8. Kammerer, R. A., Kostrewa, D., Zurdo, J., Detken, A., Garcia-Echeverria, C., Green, J. D., Muller, S. A., Meier, B. H., Winkler, F. K., Dobson, C. M., and Steinmetz, M. O. (2004) Exploring amyloid formation by a *de novo* design, *Proc. Natl. Acad. Sci. U.S.A. 101*, 4435−4440.

9. Sipe, J. D. (1992) Amyloidosis, *Annu. Rev. Biochem. 61*, 947−975.

10. Sipe, J. D., and Cohen, A. S. (2000) Review: History of the amyloid fibril, *J. Struct. Biol. 130*, 88−98.

11. Klein, W. L., Stine, W. B., Jr., and Teplow, D. B. (2004) Small assemblies of unmodified amyloid β-protein are the proximate neurotoxin in Alzheimer's disease, *Neurobiol. Aging 25*, 569−580.

12. Kirkitadze, M. D., Bitan, G., and Teplow, D. B. (2002) Paradigm shifts in Alzheimer's disease and other neurodegenerative disorders: The emerging role of oligomeric assemblies, *J. Neurosci. Res. 69*, 567−577.

13. Walsh, D. M., Hartley, D. M., Kusumoto, Y., Fezoui, Y., Condron, M. M., Lomakin, A., Benedek, G. B., Selkoe, D. J., and Teplow, D. B. (1999) Amyloid β-protein fibrillogenesis: Structure and biological activity of protofibrillar intermediates, *J. Biol. Chem. 274*, 25945−25952.

14. Walsh, D. M., Lomakin, A., Benedek, G. B., Condron, M. M., and Teplow, D. B. (1997) Amyloid β-protein fibrillogenesis: Detection of a protofibrillar intermediate, *J. Biol. Chem. 272*, 22364−22372.

15. Harper, J. D., Wong, S. S., Lieber, C. M., and Lansbury, P. T. (1997) Observation of metastable $A\beta$ amyloid protofibrils by atomic force microscopy, *Chem. Biol. 4*, 119−125.

16. Bitan, G., Kirkitadze, M. D., Lomakin, A., Vollers, S. S., Benedek, G. B., and Teplow, D. B. (2003) Amyloid β-protein ($A\beta$) assembly: $A\beta 40$ and $A\beta 42$ oligomerize through distinct pathways, *Proc. Natl. Acad. Sci. U.S.A. 100*, 330−335.

17. Oda, T., Wals, P., Osterburg, H. H., Johnson, S. A., Pasinetti, G. M., Morgan, T. E., Rozovsky, I., Stine, W. B., Snyder, S. W., Holzman, T. F., Krafft, G. A., and Finch, C. E. (1995) Clusterin (ApoJ) alters the aggregation of amyloid β-peptide ($A\beta_{1-42}$) and forms slowly sedimenting $A\beta$ complexes that cause oxidative stress, *Exp. Neurol. 136*, 22−31.

18. Lambert, M. P., Barlow, A. K., Chromy, B. A., Edwards, C., Freed, R., Liosatos, M., Morgan, T. E., Rozovsky, I., Trommer, B., Viola, K. L., Wals, P., Zhang, C., Finch, C. E., Krafft, G. A., and Klein, W. L. (1998) Diffusible, nonfibrillar ligands derived from $A\beta_{1-42}$ are potent central nervous system neurotoxins, *Proc. Natl. Acad. Sci. U.S.A. 95*, 6448−6453.

19. Walsh, D. M., Klyubin, I., Fadeeva, J. V., Cullen, W. K., Anwyl, R., Wolfe, M. S., Rowan, M. J., and Selkoe, D. J. (2002) Naturally secreted oligomers of amyloid β protein potently inhibit hippocampal long-term potentiation *in vivo*, *Nature 416*, 535−539.

20. Westlind-Danielsson, A., and Arnerup, G. (2001) Spontaneous in vitro formation of supramolecular β-amyloid structures, "βamyballs," by β-amyloid 1−40 peptide, *Biochemistry 40*, 14736−14743.

21. Hoshi, M., Sato, M., Matsumoto, S., Noguchi, A., Yasutake, K., Yoshida, N., and Sato, K. (2003) Spherical aggregates of β-amyloid (amylospheroid) show high neurotoxicity and activate tau protein kinase I/glycogen synthase kinase-3β, *Proc. Natl. Acad. Sci. U.S.A. 100*, 6370−6375.

22. Gong, Y., Chang, L., Viola, K. L., Lacor, P. N., Lambert, M. P., Finch, C. E., Krafft, G. A., and Klein, W. L. (2003) Alzheimer's disease-affected brain: Presence of oligomeric $A\beta$ ligands (ADDLs) suggests a molecular basis for reversible memory loss, *Proc. Natl. Acad. Sci. U.S.A. 100*, 10417−10422.

23. Pitschke, M., Prior, R., Haupt, M., and Riesner, D. (1998) Detection of single amyloid β-protein aggregates in the cerebrospinal fluid of Alzheimer's patients by fluorescence correlation spectroscopy, *Nat. Med. 4*, 832−834.

24. Klein, W. L. (2002) $A\beta$ toxicity in Alzheimer's disease: Globular oligomers (ADDLs) as new vaccine and drug targets, *Neurochem. Int. 41*, 345−352.

25. Klein, W. L. (2002) ADDLs & protofibrils: The missing links? *Neurobiol. Aging 23*, 231−233.

26. Klein, W. L., Krafft, G. A., and Finch, C. E. (2001) Targeting small $A\beta$ oligomers: The solution to an Alzheimer's disease conundrum? *Trends Neurosci. 24*, 219−224.

27. Serpell, L. C. (2000) Alzheimer's amyloid fibrils: Structure and assembly, *Biochim. Biophys. Acta 1502*, 16−30.

28. Fezoui, Y., and Teplow, D. B. (2002) Kinetic studies of amyloid β-protein fibril assembly: Differential effects of α-helix stabilization, *J. Biol. Chem. 277*, 36948−36954.

29. Kirkitadze, M. D., Condron, M. M., and Teplow, D. B. (2001) Identification and characterization of key kinetic intermediates in amyloid β-protein fibrillogenesis, *J. Mol. Biol. 312*, 1103−1119.

30. Soto, C., Castaño, E. M., Frangione, B., and Inestrosa, N. C. (1995) The α-helical to β-strand transition in the amino-terminal fragment of the amyloid β-peptide modulates amyloid formation, *J. Biol. Chem. 270*, 3063−3067.

31. Halverson, K., Fraser, P. E., Kirschner, D. A., and Lansbury, P. T., Jr. (1990) Molecular determinants of amyloid deposition in Alzheimer's disease: Conformational studies of synthetic β-protein fragments, *Biochemistry 29*, 2639−2644.

32. Shao, H. Y., Jao, S. C., Ma, K., and Zagorski, M. G. (1999) Solution structures of micelle-bound amyloid β-(1−40) and β-(1−42) peptides of Alzheimer's disease, *J. Mol. Biol. 285*, 755−773.

33. Zagorski, M. G., and Barrow, C. J. (1992) NMR studies of amyloid β-peptides: Proton assignments, secondary structure, and mechanism of an α-helix → β-sheet conversion for a homologous, 28-residue, N-terminal fragment, *Biochemistry 31*, 5621−5631.

34. Jarvet, J., Damberg, P., Bodell, K., Göran Eriksson, L. E., and Gräslund, A. (2000) Reversible random coil to β-sheet transition and the early stage of aggregation of the $A\beta(12-28)$ fragment from the Alzheimer peptide, *J. Am. Chem. Soc. 122*, 4261−4268.

35. Yang, D. S., Yip, C. M., Huang, T. H. J., Chakrabartty, A., and Fraser, P. E. (1999) Manipulating the amyloid-β aggregation pathway with chemical chaperones, *J. Biol. Chem. 274*, 32970–32974.

36. Janek, K., Rothemund, S., Gast, K., Beyermann, M., Zipper, J., Fabian, H., Bienert, M., and Krause, E. (2001) Study of the conformational transition of Aβ(1–42) using D-amino acid replacement analogues, *Biochemistry 40*, 5457–5463.

37. Volles, M. J., and Lansbury, P. T. (2003) Zeroing in on the pathogenic form of α-synuclein and its mechanism of neurotoxicity in Parkinson's disease, *Biochemistry 42*, 7871–7878.

38. Uversky, V. N., and Fink, A. L. (2004) Conformational constraints for amyloid fibrillation: The importance of being unfolded, *Biochim. Biophys. Acta 1698*, 131–153.

39. Lakowicz, J. R. (1999) *Principles of fluorescence spectroscopy*, 2nd ed., Kluwer Academic/Plenum Publishers, New York.

40. Ross, J. B. A., Laws, W. R., Rousslang, K. W., and Wyssbrod, H. R. (1992) in *Topics in fluorescence spectroscopy* (Lakowicz, J. R., Ed.) pp 1–63, Plenum Press, New York.

41. Cowgil, R. W. (1976) in *Biochemical Fluorescence* (Chen, R. F., and Edelhoch, H., Eds.) pp 441–486, Marcel Dekker, New York.

42. Fezoui, Y., Hartley, D. M., Harper, J. D., Khurana, R., Walsh, D. M., Condron, M. M., Selkoe, D. J., Lansbury, P. T., Fink, A. L., and Teplow, D. B. (2000) An improved method of preparing the amyloid β-protein for fibrillogenesis and neurotoxicity experiments, *Amyloid: Int. J. Exp. Clin. Invest. 7*, 166–178.

43. Jao, S. C., Ma, K., Talafous, J., Orlando, R., and Zagorski, M. G. (1997) Trifluoroacetic acid pretreatment reproducibly disaggregates the amyloid β-peptide, *Amyloid: Int. J. Exp. Clin. Invest. 4*, 240–252.

44. Zagorski, M. G., Yang, J., Shao, H., Ma, K., Zeng, H., and Hong, A. (1999) Methodological and chemical factors affecting amyloid-β peptide amyloidogenicity, *Methods Enzymol. 309*, 189–204.

45. Dahlgren, K. N., Manelli, A. M., Stine, W. B., Jr., Baker, L. K., Krafft, G. A., and LaDu, M. J. (2002) Oligomeric and fibrillar species of amyloid-β peptides differentially affect neuronal viability, *J. Biol. Chem. 277*, 32046–32053.

46. Stine, W. B., Dahlgren, K. N., Krafft, G. A., and LaDu, M. J. (2003) In vitro characterization of conditions for amyloid-β peptide oligomerization and fibrillogenesis, *J. Biol. Chem. 278*, 11612–11622.

47. LeVine, H., III (2004) Alzheimer's β-peptide oligomer formation at physiologic concentrations, *Anal. Biochem. 335*, 81–90.

48. Ezra, D., Castillo, U. F., Strobel, G. A., Hess, W. M., Porter, H., Jensen, J. B., Condron, M. A., Teplow, D. B., Sears, J., Maranta, M., Hunter, M., Weber, B., and Yaver, D. (2004) Coronamycins, peptide antibiotics produced by a verticillate *Streptomyces* sp. (MSU-2110) endophytic on *Monstera* sp., *Microbiology 150*, 785–793.

49. Byler, D. M., and Susi, H. (1986) Examination of the secondary structure of proteins by deconvolved FTIR spectra, *Biopolymers 25*, 469–487.

50. Yang, P. W., Mantsch, H. H., Arrondo, J. L., Saint-Girons, I., Guillou, Y., Cohen, G. N., and Barzu, O. (1987) Fourier transform infrared investigation of the *Escherichia coli* methionine apo-repressor, *Biochemistry 26*, 2706–2711.

51. Schmid, F. X. (1989) in *Protein structure: A practical approach* (Creighton, T. E., Ed.) pp 251–285, IRL Press, New York.

52. Dayhoff, M. O., Barker, W. C., and Hunt, L. T. (1983) Establishing homologies in protein sequences, *Methods Enzymol. 91*, 524–545.

53. Petkova, A. T., Ishii, Y., Balbach, J. J., Antzutkin, O. N., Leapman, R. D., Delaglio, F., and Tycko, R. (2002) A structural model for Alzheimer's β-amyloid fibrils based on experimental constraints from solid-state NMR, *Proc. Natl. Acad. Sci. U.S.A. 99*, 16742–16747.

54. Riek, R., Guntert, P., Döbeli, H., Wipf, B., and Wüthrich, K. (2001) NMR studies in aqueous solution fail to identify significant conformational differences between the monomeric forms of two Alzheimer peptides with widely different plaque-competence, Aβ-(1–40)ox and Aβ(1–42)ox, *Eur. J. Biochem. 268*, 5930–5936.

55. Garzon-Rodriguez, W., Vega, A., Sepulveda-Becerra, M., Milton, S., Johnson, D. A., Yatsimirsky, A. K., and Glabe, C. G. (2000) A conformation change in the carboxyl terminus of Alzheimer's Aβ(1–40) accompanies the transition from dimer to fibril as revealed by fluorescence quenching analysis, *J. Biol. Chem. 275*, 22645–22649.

56. Török, M., Milton, S., Kayed, R., Wu, P., McIntire, T., Glabe, C., and Langen, R. (2002) Structural and dynamic features of Alzheimer's Aβ peptide in amyloid fibrils studied by site-directed spin labeling, *J. Biol. Chem. 277*, 40810–40815.

57. Urbanc, B., Cruz, L., Yun, S., Ding, F., Buldyrev, S. V., Bitan, G., Teplow, D. B., and Stanley, H. E. (2004) *In silico* study of amyloid β-protein folding and oligomerization, *Proc. Natl. Acad. Sci. U.S.A. 101*, 17345–17350.

58. Tarus, B., Straub, J. E., and Thirumalai, D. (2005) Probing the initial stage of aggregation of the Aβ10−35-protein: Assessing the propensity for peptide dimerization, *J. Mol. Biol. 345*, 1141–1156.

59. Searcy, D. G., Montenay-Garestier, T., and Helene, C. (1989) Phenylalanine-to-tyrosine singlet energy transfer in the archaebacterial histone-like protein HTa, *Biochemistry 28*, 9058–9065.

60. McGuire, R., and Feldman, I. (1973) The quenching of tyrosine and tryptophan fluorescence by H2O and D2O, *Photochem. Photobiol. 18*, 119–124.

61. Froehlich, P. M., and Yeats, M. (1976) The effect of mixed aqueous solvent systems on the fluorescence of indoles and aromatic amino acids and their metabolites, *Anal. Chim. Acta 87*, 185–191.

62. Edelhoch, H., Bernstein, R. S., and Wilchek, M. (1968) The fluorescence of tyrosyl and tryptophanyl diketopiperazines, *J. Biol. Chem. 243*, 5985–5992.

63. Timasheff, S. N., and Gorbunoff, M. J. (1967) Conformation of proteins, *Annu. Rev. Biochem. 36*, 13–54.

64. Lehrer, S. S. (1976) in *Biochemical Fluorescence* (Chen, R. F., and Edelhoch, H., Eds.) pp 515–544, Marcel Dekker, New York.

65. Byerly, D. W., McElroy, C. A., and Foster, M. P. (2002) Mapping the surface of *Escherichia coli* peptide deformylase by NMR with organic solvents, *Protein Sci. 11*, 1850–1853.

66. Arrondo, J. L., Muga, A., Castresana, J., and Goni, F. M. (1993) Quantitative studies of the structure of proteins in solution by Fourier-transform infrared spectroscopy, *Prog. Biophys. Mol. Biol. 59*, 23–56.

67. Haris, P. I., and Chapman, D. (1995) The conformational analysis of peptides using Fourier transform IR spectroscopy, *Biopolymers 37*, 251–263.

68. Surewicz, W. K., and Mantsch, H. H. (1989) The conformation of dynorphin A-(1–13) in aqueous solution as studied by Fourier transform infrared spectroscopy, *J. Mol. Struct. 214*, 143–147.

69. Bitan, G., Vollers, S. S., and Teplow, D. B. (2003) Elucidation of primary structure elements controlling early amyloid β-protein oligomerization, *J. Biol. Chem. 278*, 34882–34889.

70. Hardy, J., and Selkoe, D. J. (2002) The amyloid hypothesis of Alzheimer's disease: Progress and problems on the road to therapeutics, *Science 297*, 353–356.

71. Bitan, G., Lomakin, A., and Teplow, D. B. (2001) Amyloid β-protein oligomerization: Prenucleation interactions revealed by photo-induced cross-linking of unmodified proteins, *J. Biol. Chem. 276*, 35176–35184.

72. Hou, L., Shao, H., Zhang, Y., Li, H., Menon, N. K., Neuhaus, E. B., Brewer, J. M., Byeon, I.-J. L., Ray, D. G., Vitek, M. P., Iwashita, T., Makula, R. A., Przybyla, A. B., and Zagorski, M. G. (2004) Solution NMR studies of the Aβ(1–40) and Aβ(1–42) peptides establish that the Met35 oxidation state affects the mechanism of amyloid formation, *J. Am. Chem. Soc. 126*, 1992–2005.

73. Wood, S. J., Wetzel, R., Martin, J. D., and Hurle, M. R. (1995) Prolines and amyloidogenicity in fragments of the Alzheimer's peptide β/A4, *Biochemistry 34*, 724–730.

74. Teplow, D. B., Lomakin, A., Benedek, G. B., Kirschner, D. A., and Walsh, D. M. (1997) in *Alzheimer's Disease: Biology, Diagnosis and Therapeutics* (Iqbal, K., Winblad, B., Nishimura, T., Takeda, M., and Wisniewski, H. M., Eds.) pp 311–319, John Wiley & Sons, Chichester, England.

75. Zhang, S., Iwata, K., Lachenmann, M. J., Peng, J. W., Li, S., Stimson, E. R., Lu, Y., Felix, A. M., Maggio, J. E., and Lee, J. P. (2000) The Alzheimer's peptide Aβ adopts a collapsed coil structure in water, *J. Struct. Biol. 130*, 130–141.

76. Kusumoto, Y., Lomakin, A., Teplow, D. B., and Benedek, G. B. (1998) Temperature dependence of amyloid β-protein fibrillization, *Proc. Natl. Acad. Sci. U.S.A. 95*, 12277–12282.

77. Lazo, N. D., Grant, M. A., Condron, M. C., Rigby, A. C., and Teplow, D. B. (2005) On the nucleation of amyloid β-protein monomer folding, *Protein Sci. 14*, 1581–1596.

78. Borreguero, J. M., Urbanc, B., Lazo, N. D., Buldyrev, S. V., Teplow, D. B., and Stanley, H. E. (2005) Folding events in the 21−30 region of amyloid β-protein (Aβ) studied *in silico*, *Proc. Natl. Acad. Sci. U.S.A. 102*, 6015−6020.

79. Hilbich, C., Kisters-Woike, B., Reed, J., Masters, C. L., and Beyreuther, K. (1991) Aggregation and secondary structure of synthetic amyloid βA4 peptides of Alzheimer's disease, *J. Mol. Biol. 218*, 149−163.

80. Antzutkin, O. N., Balbach, J. J., Leapman, R. D., Rizzo, N. W., Reed, J., and Tycko, R. (2000) Multiple quantum solid-state NMR indicates a parallel, not antiparallel, organization of β-sheets in Alzheimer's β-amyloid fibrils, *Proc. Natl. Acad. Sci. U.S.A. 97*, 13045−13050.